Revealing and attenuating the electrostatic properties of tubulin and its polymers.

Aarat P. Kalra, Sahil D. Patel, Boden B. Eakins, Saralyn Riddell, Pawan Kumar, Philip Winter, Jordane Preto, Kris W. Carlson, John D. Lewis, Vahid Rezania, Jack A. Tuszyński, Karthik Shankar *

A.P.K, S.D.P, B.B.E, Prof. J.A.T
Department of Physics, University of Alberta, 11335 Saskatchewan Dr NW, Edmonton, Alberta T6G 2M9, Canada

S.R, Dr. P.K, Prof. K.S
Department of Electrical and Computer Engineering, University of Alberta, 9107–116 St, Edmonton, Alberta T6G 2V4, Canada

P.W, Prof. J.D.L
Department of Oncology, University of Alberta, Edmonton, Alberta, T6G 1Z2, Canada

Dr. J.P
Centre de Recherche en Cancérologie de Lyon, INSERM 1052, CNRS 5286, Université Claude Bernard Lyon 1, Lyon, France

Dr. K.W.C
Department of Neurosurgery, Beth Israel Deaconess Medical Centre, Harvard Medical School, Boston, MA, USA

Prof. V.R
Department of Physical Sciences, MacEwan University, Edmonton, Alberta, T5J 4S2, Canada.

E-mail: kshankar@ualberta.ca

Prof. K.S
Department of Electrical and Computer Engineering, University of Alberta, 9107–116 St, Edmonton, Alberta T6G 2V4, Canada

Keywords: tubulin, electric charge, protein mobility, zeta potential, solvent sensor, dimethyl sulfoxide

Abstract

Tubulin is an electrostatically negative protein that forms cylindrical polymers termed microtubules, which are crucial for a variety of intracellular roles. Exploiting the electrostatic behaviour of tubulin and microtubules within functional microfluidic and optoelectronic devices is limited due to the lack of understanding of tubulin behavior as a function of solvent composition. This work displays the tunability of tubulin surface charge using DMSO for the first time. Increasing the DMSO volume fractions leads to the lowering of tubulin's negative

surface charge, eventually causing it to become positive in solutions > 80 % DMSO. As determined by electrophoretic mobility measurements, this change in surface charge is directionally reversible i.e. permitting control between –1.5 $cm^2 (V\ s)^{-1}$ and + 0.2 $cm^2 (V\ s)^{-1}$. When usually negative microtubules are exposed to these conditions, the positively charged tubulin forms tubulin sheets and aggregates, as revealed by an electrophoretic transport assay. Fluorescence-based experiments also indicate that tubulin sheets and aggregates co-localize with negatively charged g-C_3N_4 sheets while microtubules do not, further verifying the presence of a positive surface charge. This study illustrates that tubulin and its polymers, in addition to being mechanically robust, are also electrically tunable.

Main text

Tubulin is a globular protein that forms hollow, cylindrical polymers termed microtubules, which play a variety of intracellular roles such as providing a mechanical force for mitotic chromosomal segregation, serving as substrates for molecular motors that drive active macromolecular transport and working synergistically with actin filaments in neuronal growth cones to drive neurite outgrowth and migration. [1-4] Microtubule mechanical properties (Young's modulus ~1 GPa; persistence length 1-10 mm [5-8]) and ability to generate forces of up to 5 pN due to polymerization [9] are key features that enable such roles, and have led to utilization within engineered nano- and micro-electromechanical systems (NEMS/MEMS). In tandem with molecular motors, microtubules have been employed within high efficiency rectifiers, [10, 11] biosensors, [12-14] direction-specific sorters and transporters, [15-18] force-meters, [19] as nanopatterning agents, [20-22] and even for parallel nanocomputing. [23] Interestingly, in addition to such mechanical roles, microtubule-based systems can also exploit the highly negative charge (47 e^-) that tubulin dimers exhibit at physiological pH values. [24, 25] This high negative charge leads to extensive counterionic condensation on the microtubule outer surface. [26-28] Experiments have validated computational predictions that

the presence of microtubules increases solution capacitance under physiologically relevant ionic conditions. [28, 29] When exposed to a.c. electric fields (in the kHz regime), these condensed counterions are modelled to contribute to imaginary impedance of the system, leading to experimentally observable frequency-specific changes in solution conductance. [30-32] The high negative charge of tubulin also leads to a large protein dipole moment because ~ 40% of the total negative charge is accumulated on the filamentous C-termini 'tails' (**Figure 1a**), which contributes to the dipole moment of the dimer when a counter ionic double layer is formed around these charges. Depending on the tubulin isotype, the value of the dimer's dipole moment ranges between 1500 D and 3500 D. [33] Upon exposure to electrical nanosecond pulses, C-termini tails are modelled to undergo conformational changes that can attenuate microtubule assembly. [34] The electrical properties of tubulin enable unprecedented control over microtubule trajectories, allowing for directed spatial migration, [35-38] and full-circle electro-rotation [39, 40] when subjected to d.c electric fields. Crucially, non-uniform electric fields can also sort microtubules in a mechanical stiffness-dependent manner. [41, 42] While tunability of the mechanical properties of microtubules is well demonstrated, tunability of electrical properties can enable the launch of several possible applications within electrically driven tubulin-based devices.

Herein, we report tunability of tubulin surface charge through the addition of DMSO as a co-solvent into aqueous buffer. We measure tubulin electrophoretic mobility (henceforth referred to simply as mobility) and zeta potential (ZP), to show that dissolving tubulin in increasingly large DMSO volume fractions can eventually result in a change in sign of the net electric charge on tubulin. We find that surface charge on tubulin becomes positive at >80 % DMSO (v/v) solutions. Upon investigation of tubulin polymers in these solutions, we find that microtubules (which would otherwise be negatively surface charged in aqueous buffers at neutral pH values) open-up to form two-dimensional sheets and aggregates, also acquiring a

net positive charge in the process. DMSO, which enhances tubulin polymerization [43] and oligomerization, [44] can also be used to mimic non-polar macromolecules such as lipids within the interior of the cell membrane. While the high mechanical strength of microtubules and their interesting electrical properties have allowed their utilization in several nanoscale devices, unlike several other bio-nanoparticles (such as Eumelanin, DNA and cellulose), [45-47] their utilization within OLEDs (organic light emitting diodes) and OPVs (organic photovoltaics) has not been possible due to the prevalence of DMSO as a solvent within these technologies, [48] Here, we present the first experimental study exploring the electrical properties of tubulin within DMSO and DMSO-majority solutions. In so doing, we demonstrate the utility of tubulin and its polymers within electrically-based devices. Our work shows that tubulin polymers, in addition to being mechanically robust, are also electro-morphologically tunable by the addition of DMSO.

To establish the mobility and ZP of tubulin in aqueous solutions, we used the two microtubule stabilization buffers BRB80 and MES80, in addition to a citrate-KOH buffer (C80, which uses citric acid as a buffering agent). As expected, we measured negative values for mobility and ZP of tubulin at neutral pH (Figure 1d, e). Of the three buffers we tested, we found the mobility and ZP of tubulin to be highest in BRB80 (mobility = $-0.37 \pm 0.10 \times 10^{-6}$ cm/Vs, ZP = -4.81 ± 1.31 mV), and lowest in C80 (mobility = $-1.06 \pm 0.10 \times 10^{-6}$ cm/Vs, ZP = -13.55 ± 1.37 mV) at neutral pH. Tubulin exhibited a neutral surface charge as the pH was lowered below 7, eventually becoming positively charged at pH <5 (Figure 1d, e; Figure S1). To investigate the electrical environment around the tubulin dimer as a function of the pH value, we first predicted the structure of tubulin as a function of its protonation state, subsequently using COMSOL Multiphysics 5.5 (COMSOL Inc, Burlington, MA) to simulate the static electric potential of tubulin (Figure 1f; Materials and Methods). Upon close inspection of the ZP and mobility of tubulin, we found that the isoelectric point (pI) of

dimeric tubulin was slightly above 5 in MES80 and was approximately 4.5 in C80 buffer (Figure S1). The insolubility of PIPES (buffering agent in BRB80) at low pH values prevented its use for tubulin pI determination in BRB80. Differences in mobility and ZP are explained by tubulin conformational changes due to different buffering agents, causing it to have different net surface charges in different environments. For example, tubulin dimers are possibly non-covalently cross-linked by sulfonate groups, thus PIPES (containing two sulfonate groups) is hypothesized to polymerize tubulin to a greater extent compared to MES80 (MES contains one sulfonate group). [49]

To determine how DMSO would alter tubulin's net surface charge, we dissolved tubulin in various DMSO volume fractions. Its mobility and ZP became less negative as the volume fraction of DMSO was increased, finally attaining a positive value (mobility at 99.7 % DMSO v/v = 0.18 ± 0.08 $cm^2 (V\ s)^{-1}$, ZP = 8.91 ± 4.01 mV) at >80% DMSO (Figure 1g, h). The effective charge of tubulin in this environment was calculated to be $+1.14 \pm 0.51$ *e*, as opposed to -4.14 ± 0.51 *e* in 0 % DMSO solution (calculation details displayed in Materials and Methods). This result indicates that tubulin's net surface charge could be attenuated by simply adding different volume fractions of DMSO to solution. The ability of DMSO to tune surface charge is explained by its aprotic nature and low relative permittivity, which acts to increase the pKa value of individual residues. This result has been predicted for various chemical species [50, 51] and has been experimentally validated for proteins such as BSA (bovine serum albumin) and lysozyme. [52] To validate these results for tubulin, we also measured the ZP and mobility of tubulin under increasing water (i.e. by diluting the solution) and glycerol volume fractions as controls. Glycerol is commonly used in polymerization 'cushion' buffers due to its stabilizing influence on microtubules. [53] Lowering ionic strength (altered here by increasing water volume fraction) alters microtubule growth rates, [54, 55] increases microtubule mobility [36] and alters their mechanical properties. Glycerol

is also used as a crowding agent to study the effect of macromolecules that occupy up to 40 % of the intracellular volume fraction. [56] The presence of crowding agents *in vitro* alters the structure and dynamics of proteins, [57-60] for example, significantly increasing microtubule growth and nucleation rates. [53] In the presence of 40 % glycerol, the mobility and ZP of tubulin were found to be $-0.29 \pm 0.02 \times 10^{-6}\ cm^2\ (V\ s)^{-1}$ and 20.39 ± 1.69 mV, respectively. Both glycerol and DMSO have similar relative electrical permittivity values ($\varepsilon_{dmso} = 46.7$, $\varepsilon_{glycerol} = 42.5$), which may indicate similar influence on the mobility and ZP of tubulin. However, as the glycerol volume fraction was increased, the tubulin ZP remained unchanged with increasing glycerol volume fractions (Figure 1h). Estimation of electrical properties in >50 % glycerol solutions was unreliable, possibly due to the high viscosity of the solutions, limiting the ability to compare the electrical effect of glycerol and DMSO addition to tubulin solutions. As solution viscosity increased due glycerol addition, tubulin mobility was reduced as expected (Figure 1g). Interestingly, the ionic strength (altered by increasing water volume fraction) was found not to influence tubulin ZP or mobility significantly (as demonstrated by a two-tailed t-test p-value of 0.851 on comparing 0 % and 99% water volume fraction).

To investigate if the tunability of tubulin surface by DMSO was directionally reversible, a 'mother liquor' solution composed of 1.13 μM tubulin dissolved in 99.9 % DMSO was prepared (Figure 1i). The addition of varying water volume fractions to 1 μL of this solution induced a reversal to negative mobility and ZP values (Figure 1j, 1k). When the opposite experiment was conducted, i.e. by the dilution of an aqueous mother liquor (containing negatively surface charged tubulin) using higher DMSO volume fractions, tubulin acquired a net positive surface charge. This experiment indicated that positively surface charged tubulin could be induced to have a negative surface charge, and vice versa. The tunability of tubulin remains unchanged irrespective of its solvent history, indicating the utility of tubulin as a DMSO sensor.

We next investigated the biochemical fate of microtubules (which have a negative surface charge), when exposed to >80 % DMSO solutions. To address this question, polymerization of 1:15 rhodamine-labelled tubulin into microtubules was performed in BRB80 (Materials and Methods). Microtubules were subsequently stabilized using either BRB80T (BRB80 supplemented with 200 μM paclitaxel) or using >80 % DMSOT (DMSO supplemented with 200 μM paclitaxel). When solutions stabilized in BRB80T were imaged using epi-fluorescence microscopy, long filamentous microtubules were observed, as expected (Figure 2a). However, when solutions stabilized in >80 % DMSOT were imaged, mixtures of two-dimensional tubulin sheets and tubulin aggregates were observed (Figure 2b). To investigate their surface charge, two-dimensional sheets of fluorine-doped graphitic carbon nitride (g-C_3N_4; a negatively surface charged fluorophore; zeta potential = −26.8 mV) [61] were introduced into tubulin polymer solutions. Interestingly, the g-C_3N_4 sheets co-localized to tubulin sheets in >80 % DMSOT solutions, validating the presence of a positive surface charge on tubulin (Figure 2e) under these conditions. However, microtubules in 50 % DMSOT (Figure 2c, 2d) and in BRB80T (Figure), being negatively surface charged, were not found to co-localize with g-C_3N_4 sheets. Due to similar dimensions and the relative ease of chemically conjugating tubulin, devices where carbon nanotubes (CNTs) and MTs work synergistically have also been fabricated. [62, 63] Correspondingly, this work envisages the utility of conjugating g-C_3N_4 to tubulin by co-localization, allowing the regulation of the electrical properties of g-C_3N_4 through doping with various chemical agents (including heteroatom precursors such as NH_4F, thiourea, 4-(diphenylphosphino) benzoic acid (4-DPPBA) and phosphoric acid) and it would be possible to regulate the electrical properties of tubulin through C-terminal cleavage or pH changes, and their furthermore their relative proximity to each other would be controlled through the addition of DMSOT. These findings

appear to illustrate that when microtubules are exposed to >80% DMSOT, positively surface charged two-dimensional polymers are formed (Figure 2f).

To further evaluate the sign of the tubulin polymer surface charge in >80 % DMSOT solutions, an electrophoretic migration assay was performed. Two groups of tubulin polymers, one in BRB80T and the other in >80% DMSOT, were separately exposed to d.c. electric fields between 6 and 60 V cm^{-1} intensity using platinum contacts (Figure 3a, 3b; Materials and Methods). Polymer migration *en masse* toward a specific contact was monitored using time-lapse epifluorescence microscopy. As expected, microtubules in BRB80T were found to migrate toward the positively charged contact (Figure 3e, 3f; Movie S1, Movie S2). However, tubulin polymers in >80 % DMSOT were found to behave in the opposite manner, migrating toward the negatively charged contact, validating their net positive surface charge (see Movie S3, Movie S4). This finding was validated further when the electric field direction was reversed and tubulin polymers were transported in the opposite direction (Figure 3c, 3d).

Taken together, these results illustrate the interplay between the electrostatic properties of tubulin (negative or positive surface charge) and its polymeric state (microtubules or sheets). We started out by quantifying the mobility and ZP of tubulin in physiological conditions and determining its isoelectric point in aqueous buffers used for microtubule polymerization. We subsequently used a variety of assays, including electrophoretic directional transport, to confirm a 'flip' in the sign of tubulin net surface charge in >80 % DMSO solutions. The effective charge of tubulin was tuned from $-4.14\ e$ in 0 % DMSO to $+1.14\ e$ in 99.7 % DMSO solutions. To our knowledge, this work is the first demonstration of the electrical tunability of tubulin using DMSO. By experimentally demonstrating tunability of tubulin electrostatics in DMSO, we bring this protein one step closer to utilization within the flexible optoelectronics industry, where DMSO is used as a solvent. Our experiments also reveal that

alteration of the tubulin surface charge by DMSO is directionally reversible and consistent with experimental and computational work showing that DMSO acts to increase pKa values of chemical species. [50, 51] We further show that when microtubules composed of negatively charged tubulin are introduced in such an environment, large sheets and amorphous aggregates are formed. In the presence of DMSO, in addition to becoming positively charged, tubulin also undergoes conformational changes due to solvent effects, that cause it to stabilize sheets instead of microtubules. [43, 64, 65] Sheets have a lower inter-protofilament curvature than microtubules, allowing for unpolymerized tubulin and neighboring sheets to form lateral contacts, forming larger sheets. [43, 66] This effect is also thought to take place when the solution pH is lowered. [67] The 'sheet stabilizing' action of DMSO-majority solutions may be a combination of (a) the lower ionic strength of DMSO-majority solutions and (b) the small positive charge on tubulin in these conditions, which leads to lower shielding between tubulin dimers (which would otherwise be large due to high electrostatic charge) allowing adjacent sheets to potentially laterally attach. DMSO has also previously been shown to enhance tubulin polymerization due to macromolecular crowding effects. [43] While this aspect has not been explored in the present paper, this could be an interesting and fruitful topic for future work.

Thus, we display the ability of tubulin surface charge to regulate the equilibrium tubulin polymer state by responding to changes in its chemical environment. In the future, evaluating interactions between microtubules and molecular motors in this solvent would be of great benefit in harnessing the electro-mechanical promise of these biologically-ubiquitous nanowires. Attenuating the electrostatic properties of tubulin and microtubules will alter the interactions of motors with these substrates very likely resulting in a new way of controlling their processivity. The integration of the microtubule-motor complex in DMSO-water mixtures would provide a fruitful method for tuning tubulin electrical properties, while

simultaneously modulating its polymeric state. Our work is the first critical step in this direction.

Supporting Information
Supporting Information is available from the Wiley Online Library or from the author.

Acknowledgements
This research was funded by grants from NSERC (Canada) awarded to JAT and KS, and by support from Novocure (Haifa, Israel). We thank Prof. Al Meldrum (University of Alberta), Dr. Chirag Patel (Stanford University) and Craig Peeples (University of Alberta) for useful discussions. Technical assistance from Dr. Mike Xia (NRC Canada, Edmonton) is appreciated.

Received: ((will be filled in by the editorial staff))
Revised: ((will be filled in by the editorial staff))
Published online: ((will be filled in by the editorial staff))

References
1. Cáceres, A.; Ye, B.; Dotti, C. G., *Current opinion in cell biology* **2012,** *24* (4), 547-553.
2. Dent, E. W.; Gupton, S. L.; Gertler, F. B., *Cold Spring Harbor perspectives in biology* **2011,** *3* (3), a001800.
3. Desai, A.; Mitchison, T. J., *Annual review of cell and developmental biology* **1997,** *13* (1), 83-117.
4. Grishchuk, E. L., Biophysics of microtubule end coupling at the kinetochore. In *Centromeres and Kinetochores*, Springer: 2017; pp 397-428.
5. Hawkins, T.; Mirigian, M.; Yasar, M. S.; Ross, J. L., *Journal of biomechanics* **2010,** *43* (1), 23-30.
6. Gittes, F.; Mickey, B.; Nettleton, J.; Howard, J., *The Journal of cell biology* **1993,** *120* (4), 923-934.
7. Memet, E.; Hilitski, F.; Morris, M. A.; Schwenger, W. J.; Dogic, Z.; Mahadevan, L., *Elife* **2018,** *7*, e34695.
8. Deriu, M. A.; Soncini, M.; Orsi, M.; Patel, M.; Essex, J. W.; Montevecchi, F. M.; Redaelli, A., *Biophysical journal* **2010,** *99* (7), 2190-2199.
9. Dogterom, M.; Yurke, B., *Science* **1997,** *278* (5339), 856-860.
10. Hiratsuka, Y.; Tada, T.; Oiwa, K.; Kanayama, T.; Uyeda, T. Q., *Biophysical Journal* **2001,** *81* (3), 1555-1561.
11. van den Heuvel, M. G.; Butcher, C. T.; Smeets, R. M.; Diez, S.; Dekker, C., *Nano Letters* **2005,** *5* (6), 1117-1122.
12. Fischer, T.; Agarwal, A.; Hess, H., *Nature nanotechnology* **2009,** *4* (3), 162.
13. Groß, H.; Heil, H. S.; Ehrig, J.; Schwarz, F. W.; Hecht, B.; Diez, S., *Nature nanotechnology* **2018,** *13* (8), 691-695.
14. Chaudhuri, S.; Korten, T.; Korten, S.; Milani, G.; Lana, T.; te Kronnie, G.; Diez, S., *Nano Letters* **2018,** *18* (1), 117-123. DOI 10.1021/acs.nanolett.7b03619.
15. Reuther, C.; Mittasch, M. u.; Naganathan, S. R.; Grill, S. W.; Diez, S., *Nano letters* **2017,** *17* (9), 5699-5705.
16. Lin, C.-T.; Kao, M.-T.; Kurabayashi, K.; Meyhofer, E., *Nano Letters* **2008,** *8* (4), 1041-1046.

17. Fujimoto, K.; Kitamura, M.; Yokokawa, M.; Kanno, I.; Kotera, H.; Yokokawa, R., *ACS nano* **2012,** *7* (1), 447-455.
18. Li, J.; Jia, Y.; Dong, W.; Feng, X.; Fei, J.; Li, J., *Nano letters* **2014,** *14* (11), 6160-6164.
19. Hess, H.; Howard, J.; Vogel, V., *Nano Letters* **2002,** *2* (10), 1113-1115.
20. Liu, J.-H.; Hsia, K.-C.; Yokokawa, R.; Lu, Y.-W., *Sensors and Actuators B: Chemical* **2019,** *298*, 126813.
21. Farhana, T. I.; Kaneko, T.; Yokokawa, R. In *The Cooperative Motility of Microtubules on Nano-Patterned Kinesin-1 Turf*, 2019 20th International Conference on Solid-State Sensors, Actuators and Microsystems & Eurosensors XXXIII (TRANSDUCERS & EUROSENSORS XXXIII), IEEE: **2019**; pp 1056-1058.
22. Kaneko, T.; Furuta, K. y.; Oiwa, K.; Shintaku, H.; Kotera, H.; Yokokawa, R., *Science Advances* **2020,** *6* (4), eaax7413.
23. Nicolau, D. V.; Lard, M.; Korten, T.; van Delft, F. C.; Persson, M.; Bengtsson, E.; Månsson, A.; Diez, S.; Linke, H., *Proceedings of the National Academy of Sciences* **2016,** *113* (10), 2591-2596.
24. Mershin, A.; Kolomenski, A. A.; Schuessler, H. A.; Nanopoulos, D. V., *Biosystems* **2004,** *77* (1-3), 73-85.
25. Nogales, E.; Wolf, S. G.; Downing, K. H., *Nature* **1998,** *393* (6681), 191-191. DOI 10.1038/30288.
26. Satarić, M.; Ilić, D.; Ralević, N.; Tuszynski, J. A., *European biophysics journal* **2009,** *38* (5), 637-647.
27. Sekulić, D. L.; Satarić, M. V., *Serbian Journal of Electrical Engineering* **2012,** *9* (1), 107-119.
28. Priel, A.; Ramos, A. J.; Tuszynski, J. A.; Cantiello, H. F., *Biophysical journal* **2006,** *90* (12), 4639-4643.
29. Kalra, A. P.; Patel, S. D.; Bhuiyan, A. F.; Preto, J.; Scheuer, K. G.; Mohammed, U.; Lewis, J. D.; Rezania, V.; Shankar, K.; Tuszynski, J. A., *Nanomaterials* **2020,** *10* (2), 265.
30. Santelices, I. B.; Friesen, D. E.; Bell, C.; Hough, C. M.; Xiao, J.; Kalra, A.; Kar, P.; Freedman, H.; Rezania, V.; Lewis, J. D., *Scientific reports* **2017,** *7* (1), 9594.
31. Tuszynski, J. A.; Friesen, D.; Freedman, H.; Sbitnev, V. I.; Kim, H.; Santelices, I.; Kalra, A. P.; Patel, S. D.; Shankar, K.; Chua, L. O., *Scientific Reports* **2020,** *10* (1), 1-11.
32. del Rocío Cantero, M.; Etchegoyen, C. V.; Perez, P. L.; Scarinci, N.; Cantiello, H. F., *Scientific reports* **2018,** *8* (1), 11899.
33. Tuszynski, J. A.; Carpenter, E. J.; Huzil, J. T.; Malinski, W.; Luchko, T.; Luduena, R. F., *International Journal of Developmental Biology* **2006,** *50* (2/3), 341.
34. Chafai, D. E.; Sulimenko, V.; Havelka, D.; Kubínová, L.; Dráber, P.; Cifra, M., *Advanced Materials* **2019,** *31* (39), 1903636.
35. Van den Heuvel, M.; De Graaff, M.; Lemay, S.; Dekker, C., *Proceedings of the National Academy of Sciences* **2007,** *104* (19), 7770-7775.
36. Stracke, R.; Böhm, K.; Wollweber, L.; Tuszynski, J.; Unger, E., *Biochemical and biophysical research communications* **2002,** *293* (1), 602-609.
37. Kim, T.; Kao, M.-T.; Hasselbrink, E. F.; Meyhöfer, E., *Nano Letters* **2007,** *7* (1), 211-217.
38. Van den Heuvel, M. G.; De Graaff, M. P.; Dekker, C., *Science* **2006,** *312* (5775), 910-914.
39. Minoura, I.; Muto, E., *Biophysical journal* **2006,** *90* (10), 3739-3748.
40. Uppalapati, M.; Huang, Y. M.; Jackson, T. N.; Hancock, W. O., *small* **2008,** *4* (9), 1371-1381.
41. Isozaki, N.; Ando, S.; Nakahara, T.; Shintaku, H.; Kotera, H.; Meyhöfer, E.; Yokokawa, R., *Scientific reports* **2015,** *5*, 7669.

42. Isozaki, N.; Shintaku, H.; Kotera, H.; Hawkins, T. L.; Ross, J. L.; Yokokawa, R., *Science Robotics* **2017,** *2* (10), eaan4882.
43. Algaier, J.; Himes, R. H., *Biochimica et Biophysica Acta (BBA)-Protein Structure and Molecular Enzymology* **1988,** *954*, 235-243.
44. Kalra, A. P.; Kar, P.; Preto, J.; Rezania, V.; Dogariu, A.; Lewis, J. D.; Tuszynski, J.; Shankar, K., *Nanoscale Advances* **2019**.
45. Vahidzadeh, E.; Kalra, A. P.; Shankar, K., *Biosensors and Bioelectronics* **2018,** *122*, 127-139.
46. Sheliakina, M.; Mostert, A. B.; Meredith, P., *Advanced Functional Materials* **2018,** *28* (46), 1805514.
47. Hagen, J. A.; Li, W.; Steckl, A.; Grote, J., *Applied Physics Letters* **2006,** *88* (17), 171109.
48. Kvakovszky, G.; McKim, A.; Moore, J. C., *ECS transactions* **2007,** *11* (2), 227-234.
49. WAXMAN, P. G.; DEL CAMPO, A. A.; LOWE, M. C.; HAMEL, E., *European journal of biochemistry* **1981,** *120* (1), 129-136.
50. Rossini, E.; Netz, R. R.; Knapp, E.-W., *Journal of chemical theory and computation* **2016,** *12* (7), 3360-3369.
51. Rossini, E.; Bochevarov, A. D.; Knapp, E. W., *ACS omega* **2018,** *3* (2), 1653-1662.
52. Fang, R.; Jing, H.; Chai, Z.; Zhao, G.; Stoll, S.; Ren, F.; Liu, F.; Leng, X., *Journal of nanobiotechnology* **2011,** *9* (1), 19.
53. Keates, R. A., *Biochemical and biophysical research communications* **1980,** *97* (3), 1163-1169.
54. Borisy, G.; Marcum, J.; Olmsted, J.; Murphy, D.; Johnson, K., *Annals of the New York Academy of Sciences* **1975,** *253* (1), 107-132.
55. Olmsted, J.; Borisy, G., *Biochemistry* **1973,** *12* (21), 4282-4289.
56. Ellis, R. J.; Minton, A. P., *Nature* **2003,** *425* (6953), 27-28.
57. Junker, N. O.; Vaghefikia, F.; Albarghash, A.; Höfig, H.; Kempe, D.; Walter, J.; Otten, J.; Pohl, M.; Katranidis, A.; Wiegand, S., *The Journal of Physical Chemistry B* **2019,** *123* (21), 4477-4486.
58. Roosen-Runge, F.; Hennig, M.; Zhang, F.; Jacobs, R. M.; Sztucki, M.; Schober, H.; Seydel, T.; Schreiber, F., *Proceedings of the National Academy of Sciences* **2011,** *108* (29), 11815-11820.
59. Rivas, G.; Minton, A. P., *Trends in biochemical sciences* **2016,** *41* (11), 970-981.
60. Kuznetsova, I. M.; Turoverov, K. K.; Uversky, V. N., *International journal of molecular sciences* **2014,** *15* (12), 23090-23140.
61. Kumar, P.; Boukherroub, R.; Shankar, K., *Journal of Materials Chemistry A* **2018,** *6* (27), 12876-12931.
62. Sikora, A.; Ramón-Azcón, J.; Kim, K.; Reaves, K.; Nakazawa, H.; Umetsu, M.; Kumagai, I.; Adschiri, T.; Shiku, H.; Matsue, T., *Nano letters* **2014,** *14* (2), 876-881.
63. Dinu, C. Z.; Bale, S. S.; Chrisey, D. B.; Dordick, J. S., *Advanced Materials* **2009,** *21* (10‐11), 1182-1186.
64. Haskins, K. M.; Zombola, R. R.; Boling, J. M.; Lee, Y. C.; Himes, R. H., *Biochemical and biophysical research communications* **1980,** *95* (4), 1703-1709.
65. Himes, R. H.; Burton, P. R.; Gaito, J., *Journal of Biological Chemistry* **1977,** *252* (17), 6222-6228.
66. Mozziconacci, J.; Sandblad, L.; Wachsmuth, M.; Brunner, D.; Karsenti, E., *PLoS One* **2008,** *3* (11), e3821.
67. Burton, P. R.; Himes, R. H., *The Journal of cell biology* **1978,** *77* (1), 120-133.
68. LeBel, R. G.; Goring, D. A. I., *Journal of Chemical & Engineering Data* **1962,** *7* (1), 100-101. DOI 10.1021/je60012a032.

69. Yang, L.-J.; Yang, X.-Q.; Huang, K.-M.; Jia, G.-Z.; Shang, H., *International Journal of Molecular Sciences* **2009,** *10* (3), 1261-1270.
70. Segur, J.; Association, G., *Aciscience. Org* **1953**, 1-27.
71. Ott, C.; Reiter, F.; Baumgartner, M.; Pielmeier, M.; Vogel, A.; Walke, P.; Burger, S.; Ehrenreich, M.; Kieslich, G.; Daisenberger, D., *Advanced Functional Materials* **2019,** *29* (18), 1900233.
72. Wang, Y.; Di, Y.; Antonietti, M.; Li, H.; Chen, X.; Wang, X., *Chemistry of Materials* **2010,** *22* (18), 5119-5121. DOI 10.1021/cm1019102.

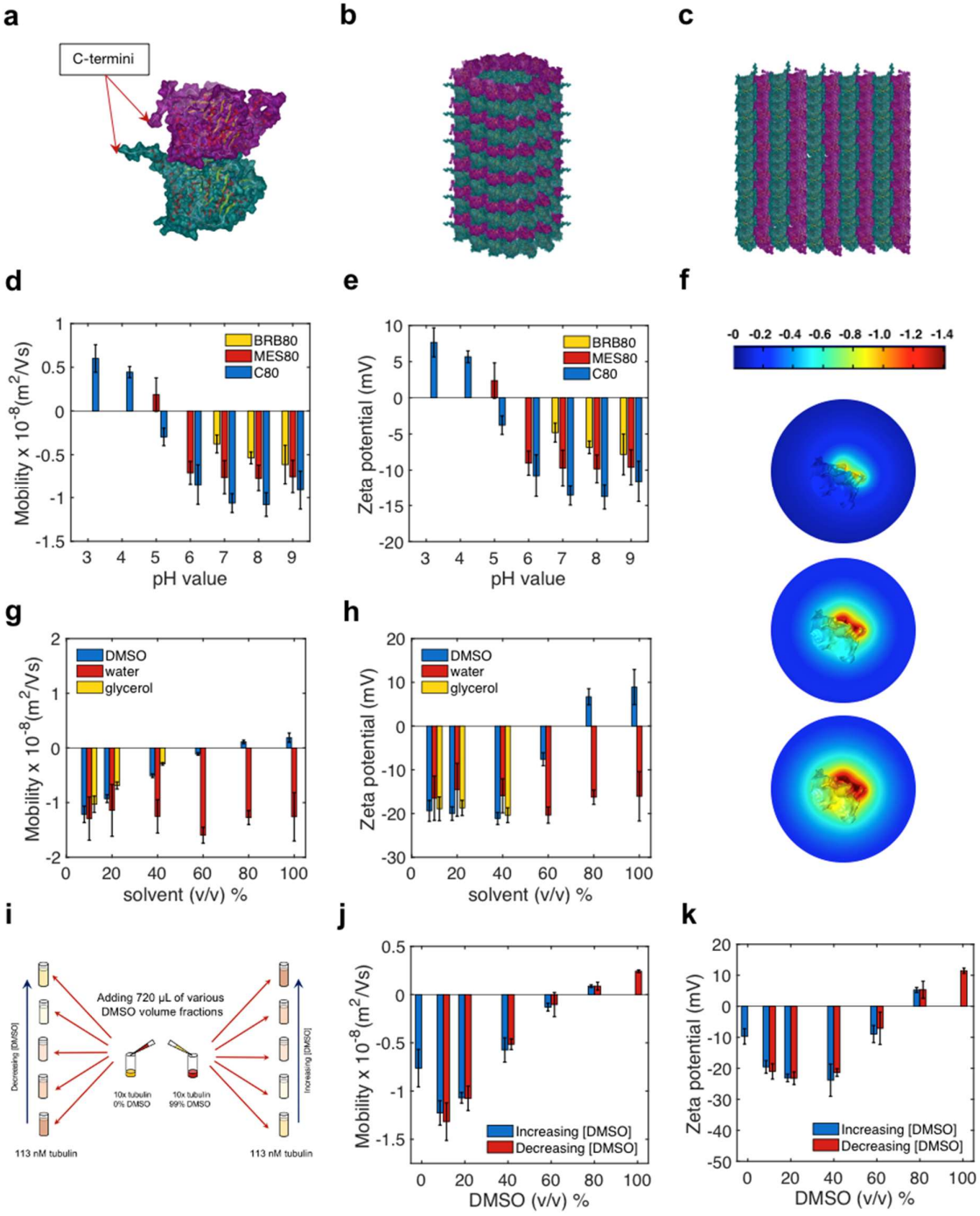

Figure 1. (a) The three-dimensional structure of the tubulin heterodimer, displaying the C-terminal tails. α and β subunits are shown in cyan and magenta respectively. (b) A schematic of the microtubule structure, composed of α, β tubulin dimers. (c) A schematic of α, β tubulin sheet structure. (d) The variation of mobility as a function of solution pH value. (e) The variation of zeta potential as a function of solution pH value. Mobility and zeta potential were measured using commercial equipment (Malvern Zetasizer; see Supporting Information). (f) A simulation of the electric potential around the tubulin dimer under varying ionic environments ranging from pH 5, to pH 7, and pH 9. Simulation was performed as described using parameters extracted from Table S1 and section S1. (g) The variation of mobility as a function of solvent volume fraction. Volume fractions were measured in percent values, with the remainder

consisting of MES80. (h) Graph displaying the variation of zeta potential as a function of solvent volume fraction. (i) The experimental procedure used to create increasing and decreasing DMSO volume fractions for probing directional reversibility. (j) Graph displaying the variation of mobility as a function of DMSO volume fraction and dilution direction. (k) Graph displaying the variation of zeta potential as a function of DMSO volume fraction and dilution direction. All measurements were performed at 25 °C.

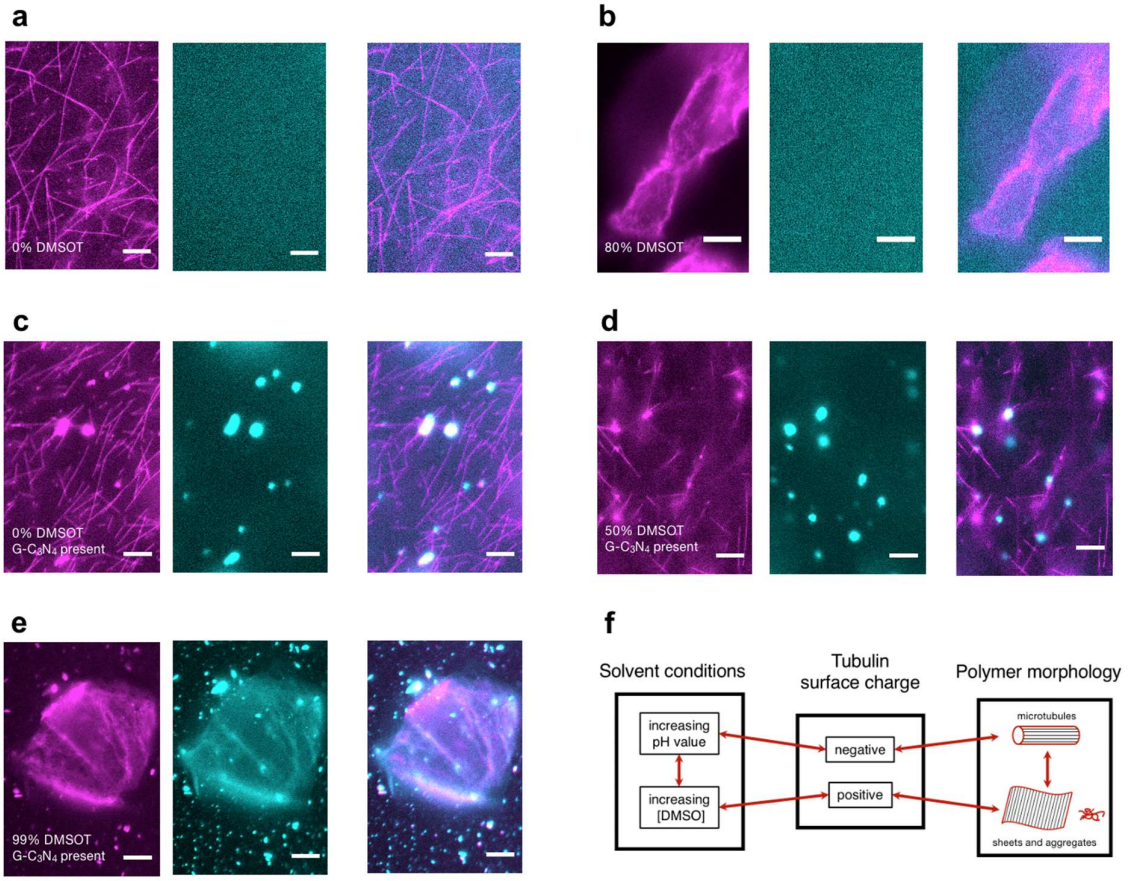

Figure 2. (a) Microtubules (450 nM tubulin) stabilized with BRB80T (0 % DMSOT), imaged with an epi-fluorescence microscope using two channels: Magenta (excitation and emission wavelengths of 535 nm and 610 nm) and Teal (excitation and emission wavelengths of 350 nm and 460 nm). (b) Microtubules (450 nM tubulin) stabilized with 80 % DMSOT. (c) Microtubules (450 nM tubulin) stabilized with BRB80T (0% DMSOT), with two dimensional sheets of G-C_3N_4 present. (d) Microtubules (450 nM tubulin) stabilized with 50 % DMSOT, with two dimensional sheets of G-C_3N_4 present. (e) Microtubules (450 nM tubulin) stabilized with 99 % DMSOT, with two dimensional sheets of G-C_3N_4 present. (f) Schematic displaying the interplay between solvent conditions, tubulin surface charge and tubulin polymer morphology. All scale bars represent 10 µm.

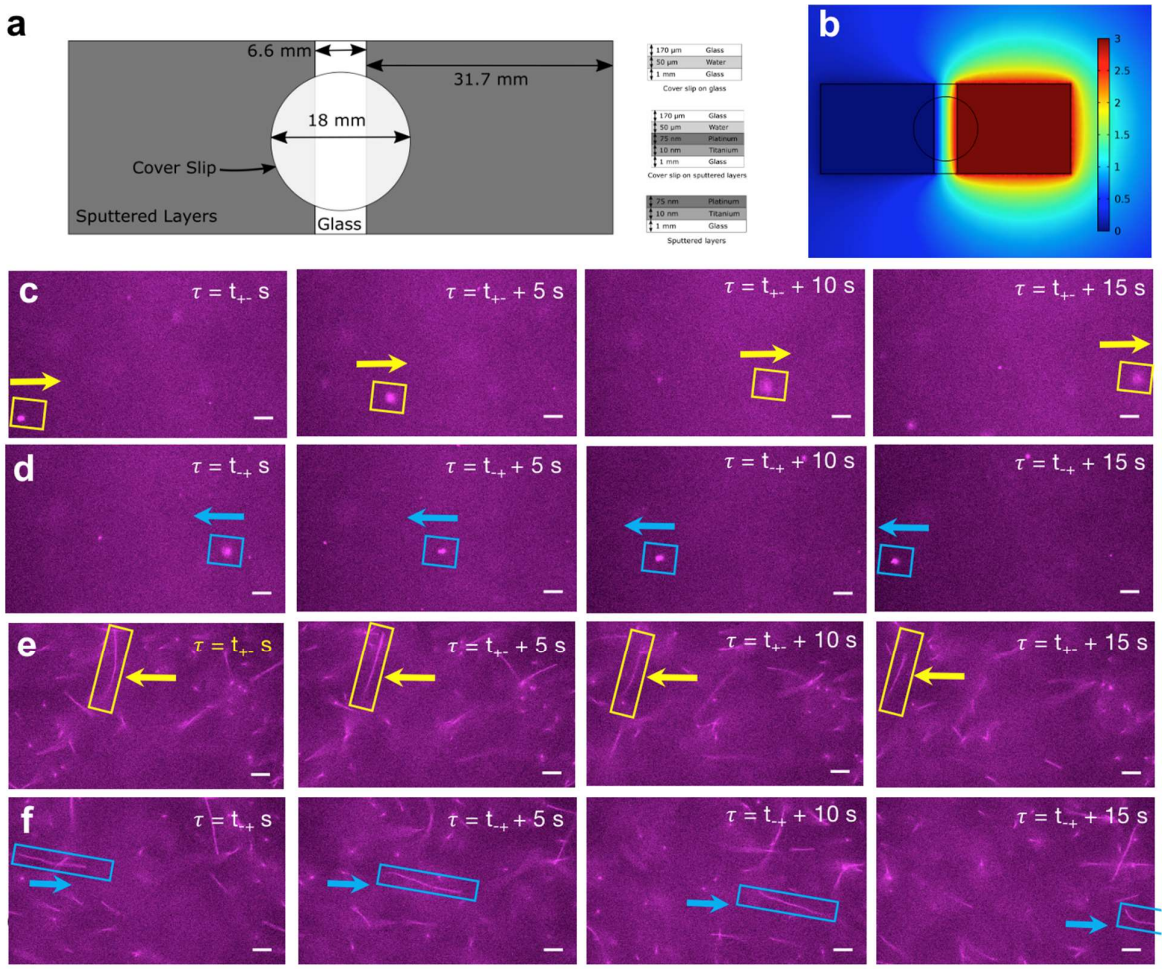

Figure 3. (a) A schematic representation of the apparatus used for the electrophoretic transport assay. (b) The electric potential values in the plane 40 nm above the glass slide. The right side of the image displays a Pt contact pad held at 3 V (resulting in an electric field intensity of 6 $V.cm^{-1}$ between the contacts), while the left side displays a grounded Pt pad. (c) An exemplary trajectory of a tubulin sheets (highlighted using a yellow box) in 98 % DMSOT, when exposed to a 24 $V.cm^{-1}$ d.c electric field in the left to right direction. (d) An exemplary trajectory of a tubulin sheets (highlighted using a blue box) in 98 % DMSOT, when exposed to a 24 $V.cm^{-1}$ d.c electric field in the right to left direction. (e) An exemplary trajectory of a microtubule when exposed to a 6 $V.cm^{-1}$ d.c electric field is in the left to right direction. The arrow indicates the direction of microtubule transport. (f) An exemplary trajectory of a microtubule (highlighted using a blue box) when exposed to a 6 $V.cm^{-1}$ d.c electric field in the right to left direction. The yellow boxes represent cases where the electric field is in the left to right direction, while the blue boxes represent opposite cases All scale bars represent 10 µm.

Controlling tubulin surface charge in a directionally reversible manner using DMSO is displayed for the first time. Mobility measurements indicate the utility of DMSO as agent to vary the tubulin surface charge in a directionally reversible manner. Microtubules form positively charged tubulin sheets and aggregates in such solutions, as illustrated by Electrophoretic transport and co-localization assays.

Keyword: tubulin charge modulation

A. P. K, S. D. P, B. B. E, S. R, Dr. P. K, P. W, Dr. J. P, Dr. K. W. C, Prof. J. D. L, Prof. V. R, Prof. J.A. T, Prof. K. S *

Revealing and attenuating the electrostatic properties of tubulin and its polymers

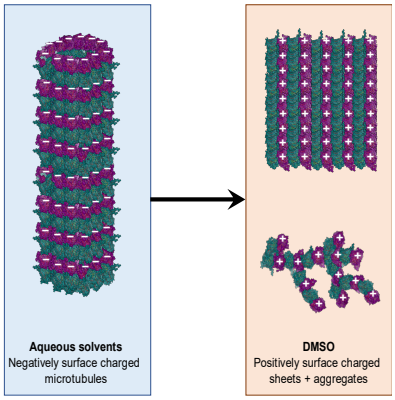

Supporting Information

Revealing and attenuating the electrostatic properties of tubulin and its polymers.

Aarat P. Kalra, Sahil D. Patel, Boden B. Eakins, Saralyn Riddell, Pawan Kumar, Philip Winter, Jordane Preto, Kris W. Carlson, John D. Lewis, Vahid Rezania, Jack A. Tuszyński, Karthik Shankar *

MATERIALS AND METHODS

S1. Simulation of electric field distribution around tubulin

A structure of a human tubulin dimer was created by homology modeling. The template structure used was 1JFF (PMID:11700061), which is bovine tubulin stabilized with a taxol ligand. 1JFF is considered to be a good structure for a tubulin dimer in a microtubule-like conformation. Sequences for human tubulin were obtained from UniProt, with Q71U36 used for alpha-tubulin and P07437 used for beta-tubulin. Sequence Q71U36 is the sequence for alpha-tubulin gene TUBA1A, which is an alpha-tubulin isotype that is highly expressed in the brain. Sequence P07437 is the sequence for beta-tubulin gene TUBB, which is a ubiquitously expressed beta-tubulin isotype. The Molecular Operating Environment (MOE; Chemical Computing Group, Montreal, Canada) was used to perform the homology modeling. The MOE loop modeler was used to generate conformations for a missing loop of the structure (alpha-tubulin positions 35-60), and for the C-terminals in both alpha-tubulin and beta-tubulin, which are highly flexible disordered regions (alpha-tubulin C-terminal was defined as positions 440-451, and beta-tubulin C-terminal was defined as positions 428-444). The best structure as determined by MOE's homology model scoring function was selected for further processing. Note that in the best scoring function structure the C-terminals had a conformation with electrostatic interactions with rest of the protein, as opposed to being extended in the solvent.
The tubulin structure thus obtained was protonated to various pH values using the 'protonate 3D' utility (solvent dielectric constant = 80 F m^{-1}; protein dielectric constant = 2 F m^{-1}; salt concentration = 0.2 M; viscosity = 0.89 × 10^{-3} Pa·s) in MOE (Molecular Operating Environment; Chemical Computing Group, Montréal, Quebéc, Canada). The final protonated structure was opened in VMD (Visual Molecular Dynamics, University of Illinois at Urbana-Champaign), and rendered to determine its surface using the 'Quicksurf' utility (grain-size = 1 unit). The resulting tubulin surface was saved and imported into SpaceClaim modeling software (SpaceClaim Corporation, Concord, Massachusetts) as a faceted body, where a 0.1 nm shrink-wrap is applied to produce an atomically correct solid body model. The tubulin surface is subsequently imported into COMSOL Multiphysics (COMSOL Inc, Burlington, MA), where the the protein is centered in a 20 nm radius spherical domain. to obtain a far-field approximation for the electrical potential profile outside the protein surface, as a function of pH value.

pH	5	7	9
Overall charge on heterodimer	-25.95 · e	-54.86 · e	-75.00 · e
Charge on α-tubulin C-terminal region	-7.38 · e	-9.24 · e	-9.31 · e
Charge on β-tubulin C-terminal region	-9.37 · e	-11.45 · e	-11.54 · e

Table S1. Charge distribution present on various regions of the tubulin heterodimer.

The region between the outer surface of the tubulin body and the and edge of the spherical domain is taken to be the computational domain. An electrical ground boundary condition is applied at the outer spherical shell, whereas the charge on the tubulin model is used as the second boundary condition.

In the calculated charge distribution of the tubulin protein, we do not account for the surface charge arising from the atomistic protein structure, instead we use a use a far-field approximation. The protein is considered as a union of two regions, the first being the main body, and the second being the 'tail-like' C-termini regions. The corresponding charges in these areas are shown in Table S1. This allows us to compute the surface charge densities on each respective region of the protein model.

$$\nabla^2 V = {}^{-\rho}/_{\epsilon_o} \qquad \text{(Equation 1)}$$

Finite element analysis is conducted in COMSOL to solve Poisson's equation (Equation 1) in the computational domain with the specified boundary conditions. Notably, the second boundary condition changes as a function of the model's surrounding chemical environment. This yields the static electric potential around the tubulin protein as shown in Figure 1f. To account for ionic screening on the electric potential as a function of distance, values of electric potential are corrected along the x-axis Debye-Hückel theory for ionic screening.

$$V_f(r) = V_i(r)e^{-r/\lambda_D} \qquad \text{(Equation 2)}$$

In Equation 2, the electric potential corrected with ionic screening is represented by $V_f(r)$, which is a function of radial distance from the protein. The un-screened electric potential is $V_i(r)$, and the Debye length is λ_D, given by eq. 3.

$$\lambda_D = \sqrt{\frac{\epsilon K_B T}{\sum_i n_i {z_i}^2}} \qquad \text{(Equation 3)}$$

In Equation 3, K_B is the Boltzmann constant, T is the temperature, ϵ represents the permittivity of the surrounding environment, n_i represents the ion species concentration, and z_i represents the charge of the corresponding ion. To match with experimental parameters, ϵ is taken to be $80\epsilon_o$, and T is taken to be 298.15 K. At every pH, Mg^{2+} and K^+ ions are present in concentrations of 1 mM and 160 mM respectively. H^+ ions are present at a concentration of 10^{-pH} M at each pH.

S2. Tubulin reconstitution, polymerization and stabilization

Lyophilized tubulin powder (Cytoskeleton Inc, Denver, CO, USA; T240) was reconstituted and with labelled tubulin (Cytoskeleton Inc, Denver, CO, USA; TL590M) as described previously [29, 44]. 45.45 μM tubulin was polymerized in a 37 °C water bath for 30 minutes in BRB80 pH 6.9 supplemented with 1 mM GTP (guanosine triphosphate; Cytoskeleton Inc, Denver, CO, USA; BST06). This step was followed by stabilization using 40 μM paclitaxel (Cytoskeleton Inc, Denver, CO, USA; TXD01; stock concentration 2mM).

S3. Determination of ZP and electrophoretic mobility using DLS

BRB80 buffers contained 80 mM PIPES, 2 mM $MgCl_2$, 0.5 mM EGTA. All MES80 buffers contained 80 mM MES, 2 mM $MgCl_2$, 0.5 mM EGTA. All C80 buffers contained 80 mM Citric

acid, 2 mM $MgCl_2$, 0.5 mM EGTA. Milli-Q water was used for all experiments. The pH value of solutions was adjusted using KOH or HCl. All mobility and ZP measurements were performed using a Malvern Zetasizer Nano ZS (Malvern Instruments, Malvern, United Kingdom). Measurements in various aqueous media was preformed using folded capillary Zeta cells (DTS1070; Malvern Instruments, Malvern, United Kingdom). The Smoluchowski approximation for a monomodal distribution of particle ZP was used to perform experiments. Tubulin (stock concentration 45.45 μM; reconstitution described above) was diluted in buffer (MES80, BRB80 or C80) to a final concentration of 113.6 nM for all experiments.
For measurements in increasing volume fractions of DMSO, glycerol and water, the ZEN1002 cell (Malvern Instruments, Malvern, United Kingdom) was used. The remaining volume fraction was composed of MES80 buffer. The dynamic viscosity, refractive index and relative permittivity used were adapted from previously published sources [68-70] and are displayed in Table S2. All measurements were conducted at 25 °C.

Solution	**DMSO or Glycerol (w/w %)**	**Dynamic viscosity (cP)**	**Refractive index (n)**	**Relative permittivity (ε_r)**
DMSO				
5 % DMSO	5.5	0.97	1.3397	78.4
10 % DMSO	11	1.084	1.3472	76.7
15 % DMSO	16.5	1.228	1.3459	75.1
20 % DMSO	22	1.404	1.3631	73.4
40 % DMSO	44	2.452	1.3977	66.7
60 % DMSO	66	3.658	1.4325	60.1
80 % DMSO	88	2.864	1.4625	53.4
99 % DMSO	108.9	1.99	1.4783	46.7
Glycerol				
5% Glycerol	1.22	1.22	1.347	75.05
10% Glycerol	1.73	1.73	1.363	71.74
20 % Glycerol	2.57	2.57	1.377	68.52
30 % Glycerol	4.05	4.05	1.391	65.33
40% Glycerol	6.86	6.86	1.406	61.68
50% Glycerol	12.76	12.76	1.420	57.62

Table S2. Table displaying the values of dynamic viscosity, refractive index and relative permittivity input for measuring the mobility of various tubulin solutions.

To investigate if negatively charged tubulin could acquire a positive charge upon the addition of increasingly large volume fractions of DMSO, solutions containing varying volume fractions of DMSO to 80 µL of '10 x tubulin' (13.6 µM protein concentration) in MES80 pH 7 solution were added. The volumes for each mixture are shown in table S3.

	DMSO	**MES buffer pH 7**	**MES80 solution 10x tubulin**
90 % DMSO	720 µL	0 µL	80 µL
80 % DMSO	640 µL	80 µL	80 µL
60 % DMSO	480 µL	240 µL	80 µL
40% DMSO	320 µL	400 µL	80 µL
20 % DMSO	160 µL	560 µL	80 µL
10 % DMSO	80 µL	640 µL	80 µL

Table S3. Volumes of solutions used for to investigate if negatively surface charged tubulin may acquire a positive charge using varying volume fractions of DMSO.

To investigate if positively charged tubulin can acquire a negative surface charge, similar experiments were performed using volumes displayed in Table S4. Importantly, the 10x tubulin solution was prepared in 99 % DMSO as a solvent. For experimental data analysis on mobility and ZP presented in this work, each experiment was performed in three sets of three experiments. Analysis was performed after combining all datapoints as one long experiment.

	DMSO	**MES buffer pH 7**	**99 % DMSO solution 10x tubulin**
99 % DMSO	720 µL	0 µL	80 µL
80 % DMSO	560 µL	160 µL	80 µL
60 % DMSO	400 µL	320 µL	80 µL
40% DMSO	240 µL	480 µL	80 µL
20 % DMSO	80 µL	640 µL	80 µL
10 % DMSO	0 µL	720 µL	80 µL

Table S4. Volumes of solutions used for to investigate if positively surface charged tubulin may acquire a negative charge using varying volume fractions of DMSO.

S4. Electrophoretic transport assay and simulation of electric field

For the electrophoretic transport assay, paclitaxel supplemented DMSO (DMSOT) was prepared by adding 5 µL of paclitaxel stock (2 mM) to 45 µL of DMSO, resulting in a final solution containing 200 µM paclitaxel. Similarly, BRB80 containing paclitaxel solutions (BRB80T) were prepared by adding 5 µL of paclitaxel stock to 45 µL of BRB80. To prepare a solution of microtubules (final concentration 450 µM tubulin), 49.5 µL of BRB80T was added to 0.5 µL of polymerized tubulin stock. To prepare microtubules (final concentration 4.5 µM tubulin) in 99 % DMSO, 49.5 µL of DMSOT was added to 0.5 µL of polymerized tubulin.

For the fabrication of contacts, sputtering of 10 nm Ti (as an adhesion layer) was performed onto a rectangular glass slide (70 mm x 25 mm x 1 mm), followed by a 75 nm thick Pt layer. The centre of the rectangular slide was covered using Kapton tape to enable the formation of

two Pt pads extending symmetrically along the long axis from the edge to 3.3 mm from the centre and along the entirety of the short axis (top view (Figure 3A); side view (Figure 3B)). A borosilicate coverslip (18 mm in diameter and 0.17 mm in thickness) was placed atop 2 µL of 450 nM tubulin polymer solution on the gap between the pads in the centre of the slide. A d.c power source was used to source this voltage. Electrophoretic flow direction was monitored using an epifluorescence microscope, using an exposure time of 100 ms, taking snapshots every 5 s for 3 minutes (Movie S1, S2, S3 and S4). During experiments, we observed that microtubules and two-dimensional tubulin polymers stuck on the surface of glass did not undergo electrophoresis even under the influence of electric fields > 24 $V.cm^{-1}$. Thus, tubulin polymers that were not stuck to the glass slide were evaluated. Cleaning of the slides after experimentation was performed with acetone and methanol rinsing, followed by five minutes exposure to oxygen plasma (Oxford Instruments, Abingdon, UK; NGP80) to remove inorganic impurities from the slide surface.

S5. Simulation of electric fields generated by Pt contacts for electrophoretic transport assay

The slide was simulated using the Electrostatics Module in COMSOL Multiphysics 5.5 as being at the centre of a sphere of air 1 m in radius. The Ti and Pt layers were computationally fabricated using the Layered Material function. The outer boundary of this sphere was specified to be ground. The surface of one of the sputtered layers of the slide was also specified to be 0 V, while the potential on the surface of the other sputtered layer was set to 3 V. The stationary state electric potential through the sphere was subsequently simulated.

S5. G-C_3N_4 and tubulin sheet co-localization fluorescence imaging

Stock G-C_3N_4 solution in water or DMSO was prepared by mixing 0.026 g of G-C_3N_4 powder [71, 72] in 5 mL water and DMSO. To investigate co-localization between G-C_3N_4 and tubulin-polymers in 99 % DMSO solutions, 0.5 µL of tubulin stock solution (Section S2) was added to 20 µL of DMSOT. This was followed by the addition of 30 µL of G-C_3N_4 solution. The 50 % DMSOT solution was prepared by adding 30 µL of G-C_3N_4 solution prepared in water and 19.5 µL of DMSOT to 2 uL of polymerized Rhodamine-labelled tubulin stock solution. The 0 % DMSO solution was prepared by adding 30 µL of G-C_3N_4 solution prepared in water and 19.5 µL of BRB80T to 2 uL of 45.45 µM polymerized Rhodamine-labelled tubulin stock solution. G-C_3N_4 solutions were sonicated in a water bath for 30 minutes before adding to tubulin solutions.

S6. Calculation of effective charge of tubulin in DMSO containing solutions

To determine the effective charge of tubulin from ZP values, tubulin was approximated as a charged sphere. Thus, the potential was determined using Equation 4 below:

$$ZP = \frac{Q}{4\pi\varepsilon_0\varepsilon_r} \qquad \text{(Equation 4)}$$

Here, Q is the effective charge of tubulin, while ZP represents zeta potential. $\varepsilon_0$and $\varepsilon_r$are the permittivity of free space and relative permittivity. In the case of 99 % DMSO solutions, the value ε_r of was assumed to be 46.7, in accordance with values shown in Table S2. In the 0 % DMSO solution case, the value of ε_r was assumed to be 78.2.

DYNAMIC LIGHT SCATTERING

To ensure that we had no initial aggregates in these 'starting point' solutions, we measured the hydrodynamic diameter of tubulin (1.13 µM) using DLS (Dynamic Light Scattering). As

expected, we found that the hydrodynamic diameter was 6.14 ± 1.97 nm as shown in Figure S2a. This result is consistent with values expected for unpolymerized tubulin, already reported by us in a previous publication [44]. After polymerization into microtubules, our work reports observations on solutions diluted with either (a) MES80T pH 7 (containing 0% DMSO), which led to the continued stabilization of negatively charged microtubules, or (b) 80 % DMSOT (20% MES80T), which led to the stabilization of positively charged sheets and aggregates. To compare the size distribution of tubulin polymorphs in both cases, we performed DLS on both dilutions (Figure S2b). These results showed different size distribution peaks, indicating differing polymorphic size distributions. Our results are consistent with microscopy-based data that indicate the transition of a different polymeric forms of tubulin when it becomes positively charged. Additionally, due to the positive charge of tubulin at MES80 pH 5, we also performed DLS measurements on microtubules diluted in MES80 pH 5. We found that that the size distribution matched that of 80 % DMSO, consistent with a polymorphic transition from microtubules to sheets at low pH values. The noise in Figure S2b is due to Mie scattering, that takes place due to large particles such as microtubules (> 1 um) which can be several micrometers long in our preparations.

SUPPLEMENTARY FIGURES

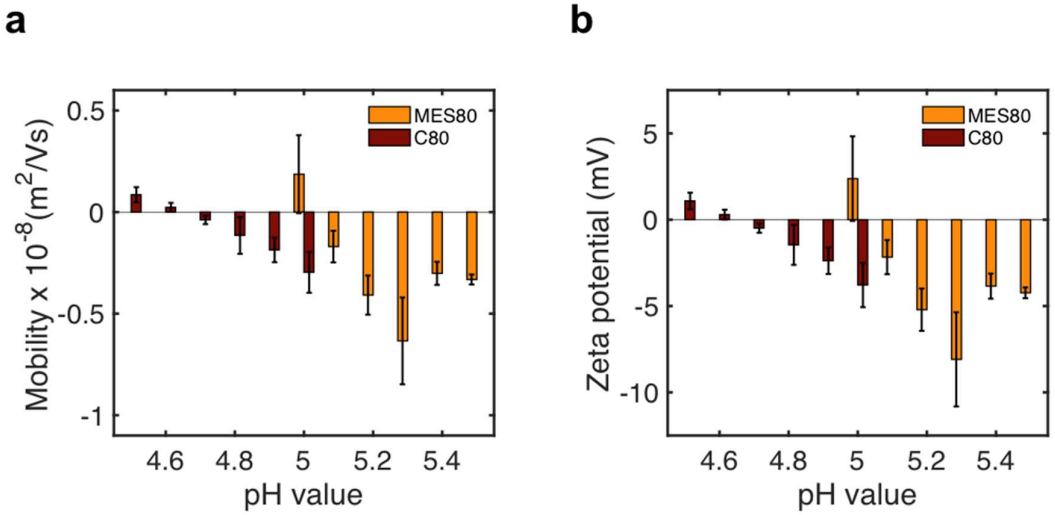

Figure S1. Graphs displaying the variation of (a) mobility and (b) zeta potential as a function of solution pH value for C80 and MES80 buffers. The isoelectric point (pI) of tubulin is approximately 4.6 in C80 and 5 in MES80.

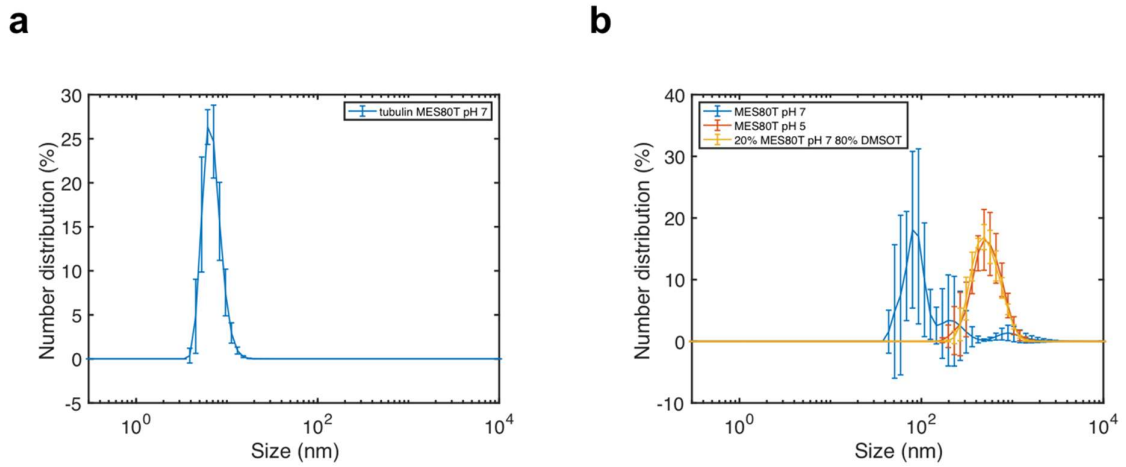

Figure S2. (a) DLS size distribution profiles of unpolymerized 1.13 µm tubulin dissolved in MES80T pH 7. (b) DLS size distribution profiles of polymerized 1.13 µm tubulin diluted in MES80T pH 7, compared to MES80T pH 5 and 80% DMSOT solutions. Error bars represent standard deviation values achieved from n = 5 measurements. The two-tailed t-test p-value of 0.0068 on comparing data from MES pH 5 and MES pH 7 shows that the difference between the two number distributions is significant. Additionally, the identical test resulted in a value of 0.0081 on comparing data from MES pH 7 and MES pH 7 with 80 % DMSO shows that the difference between the two number distributions is also significant.

SUPPLEMENTARY MOVIES

Movie S1. Movie displaying the electrophoretic transport of 4.5 µM microtubules in BRB80T, using no exposure (in frames 1-21), a 6 $V.cm^{-1}$ exposure (positive contact and negative contacts on the left and right side respectively; in frames 22-41) and a 6 $V.cm^{-1}$ exposure in the reverse direction (positive contact and negative contacts on the right and left side respectively; in frames 42-61).

Movie S2. Movie displaying the electrophoretic transport of 4.5 µM microtubules in BRB80T, using no exposure (in frames 1-21), a 6 $V.cm^{-1}$ exposure (positive contact and negative contacts on the left and right side respectively; in frames 22-41) and a 6 $V.cm^{-1}$ exposure in the reverse direction (positive contact and negative contacts on the right and left side respectively; in frames 42-61). All conditions are identical to Movie S1.

Movie S3. Movie displaying the electrophoretic transport of 4.5 µM tubulin polymers and aggregates in 80 % DMSOT, using no exposure (in frames 1-21), a 6 $V.cm^{-1}$ exposure (positive contact and negative contacts on the left and right side respectively; in frames 22-41) and a 6 $V.cm^{-1}$ exposure in the reverse direction (positive contact and negative contacts on the right and left side respectively; in frames 42-61).

Movie S4. Movie displaying the electrophoretic transport of 4.5 µM microtubules in 80 % DMSOT, using no exposure (in frames 1-21), a 60 $V.cm^{-1}$ exposure (positive contact and

negative contacts on the left and right side respectively; in frames 22-41) and a 60 $V.cm^{-1}$ exposure in the reverse direction (positive contact and negative contacts on the right and left side respectively; in frames 42-61).